Emergence of Superconductivity on the Border of Antiferromagnetic Order in $RbMn_6Bi_5$ under High Pressure: A New Family of Mn-Based Superconductors

Peng-Tao Yang(杨芃焘)[1,2†], Qing-Xin Dong(董庆新)[1,2†], Peng-Fei Shan(单鹏飞)[1,2†], Zi-Yi Liu(刘子儀)[1,2†], Jian-Ping Sun(孙建平)[1,2], Zhi-Ling Dun(顿志凌)[1,2], Yoshiya Uwatoko[3], Gen-Fu Chen(陈根富)[1,2*], Bo-Sen Wang(王铂森)[1,2*], and Jin-Guang Cheng(程金光)[1,2*]

[1]*Beijing National Laboratory for Condensed Matter Physics and Institute of Physics, Chinese Academy of Sciences, Beijing 100190, China*
[2]*School of Physical Sciences, University of Chinese Academy of Sciences, Beijing 100190, China*
[3]*Institute for Solid State Physics, University of Tokyo, Kashiwa, Chiba 277-8581, Japan*

(Received 28 March 2022; accepted 21 April 2022; published online)

We report the discovery of superconductivity on the border of antiferromagnetic order in a quasi-one-dimensional material $RbMn_6Bi_5$ via measurements of resistivity and magnetic susceptibility under high pressures. Its phase diagram of temperature versus pressure resembles those of many magnetism-mediated superconducting systems. With increasing pressure, its antiferromagnetic ordering transition with $T_{\rm N} = 83\,{\rm K}$ at ambient pressure is first enhanced moderately and then suppressed completely at a critical pressure of $P_{\rm c} \approx 13\,{\rm GPa}$, around which bulk superconductivity emerges and exhibits a dome-like $T_{\rm c}(P)$ with a maximal $T_{\rm c}^{\rm onset} \approx 9.5\,{\rm K}$ at about 15 GPa. In addition, the superconducting state around $P_{\rm c}$ is characterized by a large upper critical field $\mu_0 H_{\rm c2}(0)$ exceeding the Pauli paramagnetic limit, implying a possible unconventional paring mechanism. The present study, together with our recent work on KMn_6Bi_5 (the maximum $T_{\rm c}^{\rm onset} \approx 9.3\,{\rm K}$), makes $A{\rm Mn_6Bi_5}$ ($A =$ alkali metal) a new family of Mn-based superconductors with relatively high $T_{\rm c}$.

DOI: 10.1088/0256-307X/39/6/067401

The advances in the field of unconventional superconductivity are largely driven by the discovery of novel superconducting systems, especially those derived from the parent compounds with antiferromagnetic (AFM) order, as exemplified by the cuprates and iron-pnictide high-temperature superconductors.[1–3] The first-row (3d) transition-metal-based compounds are at the forefront of materials' discovery for unconventional superconductivity due to the presence of strong electronic correlations and the proximity to magnetic instability. In 2015, we discovered pressure-induced superconductivity in MnP with the critical temperature ($T_{\rm c}$) about 1 K by suppressing its helimagnetic order under high pressure.[4] This finding breaks the general wisdom about Mn's antagonistic to superconductivity and has thus promoted the quest for more Mn-based superconductors with higher $T_{\rm c}$. After years of explorations, we recently found that KMn_6Bi_5 with a unique quasi-one-dimensional (Q1D) structure becomes superconducting with a relatively high $T_{\rm c}^{\rm onset}$ up to 9.3 K when its antiferromagnetic order is suppressed by pressure.[5] This finding makes KMn_6Bi_5 the first *ternary* Mn-based superconductor with an optimal $T_{\rm c}$ about an order higher than that of MnP. Importantly, this result demonstrates that the $T_{\rm c}$ of Mn-based superconductors has a potential to go higher. In addition, the obtained temperature-pressure phase diagram of KMn_6Bi_5, featured by a superconducting dome on the border of antiferromagnetic order, resembles those of many unconventional superconducting systems associated with magnetism-mediated pairing mechanism.[6–8] Since KMn_6Bi_5 is one member of the Q1D $A{\rm Mn_6Bi_5}$ ($A =$ alkali metal) system,[9–11] it is natural to ask whether they consist of a new family of Mn-based superconductors. To address this issue, here we turn our attention to $RbMn_6Bi_5$.

As shown in Fig. 1(a), $RbMn_6Bi_5$ also adopts the monoclinic structure (space group $C2/m$) featured by the infinite $[Mn_6Bi_5]^-$ columns, which are composed of an outer nanotube of Bi atoms, an inner Mn–Mn bonded metallic pentagon core and a one-dimensional Mn–Mn atomic chain in the center along the b axis. The counter-cation Rb^+ ions fill the space between the $[Mn_6Bi_5]^-$ columns, acting as the structural frame and carriers' source.[9–11] Replacing K^+ with a larger radius ion Rb^+ in $A{\rm Mn_6Bi_5}$ leads to anisotropic expansions of lattice parameters, i.e., the

†These authors contributed equally to this work.
*Corresponding authors. Email: bswang@iphy.ac.cn; gfchen@iphy.ac.cn; jgcheng@iphy.ac.cn

a and c are expanded by 1.27% and 1.85%, respectively, while the b is only increased by 0.19%. This means that the $[Mn_6Bi_5]^-$ columns remain almost intact by the replacement of larger A-site cation while the intercolumn interactions are weakened, leading to a stronger anisotropy in $RbMn_6Bi_5$. At ambient pressure (AP), $RbMn_6Bi_5$ undergoes an antiferromagnetic transition at $T_N \approx 83$ K, slightly higher than that of KMn_6Bi_5 ($T_N \approx 75$ K). Around T_N, the resistivity along the rod ($\rho_{//}$) shows a weak kink while the resistivity perpendicular to the rod ($\rho_{\perp}$) exhibits a pronounced upturn. First-principles calculations indicate that the density of states at Fermi level are mainly contributed from the Mn-3d electron bands in the Mn10 pentagonal antiprisms, and the nonlinear helical spin structures, similar with MnP and $A_2Cr_3As_3$,[12–15] are found to be energetically stable.[10] In this regard, the itinerant magnetism of $RbMn_6Bi_5$ with enhanced anisotropy and relatively low T_N makes it a promising candidate for realizing unconventional superconductivity near the magnetic quantum critical point (QCP).

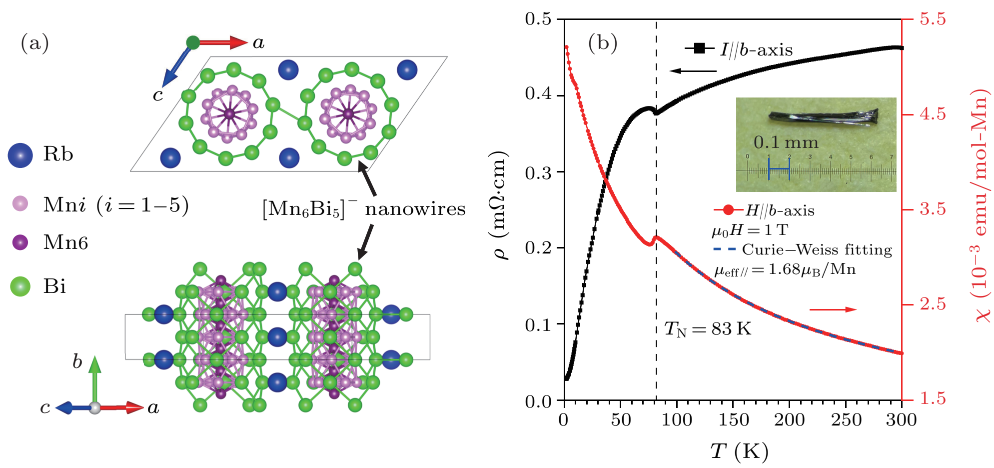

Fig. 1. (a) Crystal structure of $RbMn_6Bi_5$. (b) Temperature dependence of the resistivity and magnetic susceptibility along the rod direction of $RbMn_6Bi_5$ crystal at AP. The T_N shows the antiferromagnetic transition temperature. The Curie–Weiss fitting is shown by the broken line. Inset of (b) shows a picture of the $RbMn_6Bi_5$ crystal.

Through detailed measurements of resistivity and magnetic susceptibility at high pressures, here we show that $RbMn_6Bi_5$ becomes superconducting when its antiferromagnetic order is suppressed by pressure at a critical pressure of $P_c \approx 13$ GPa. The maximal $T_c^{onset} \approx 9.5$ K is achieved at $\sim$15 GPa. In addition, the superconducting state around P_c is characterized by a large upper critical field $\mu_0 H_{c2}(0)$ exceeding the Pauli limit, indicating a possible unconventional paring mechanism. Along with our recent work on KMn_6Bi_5,[5] the present study establish AMn_6Bi_5 as a new family of ternary Mn-based superconductors with relatively high T_c, which should be subjected to further experimental and theoretical investigations.

Experimental. $RbMn_6Bi_5$ single crystals were grown by using the Rb-Bi flux method as reported previously.[10] We measured single-crystal x-ray diffraction (XRD) at 300 K and confirmed that $RbMn_6Bi_5$ crystallizes in a monoclinic structure with space group $C2/m$. The refined lattice parameters are consistent with the previous report.[10] Energy dispersive spectroscopy (EDS) measurements on the fresh surface of crystals confirm that the average chemical composition, Rb:Mn:Bi = 1 : 6.11 : 5.08, is close to the stoichiometric ratio. Electrical transport and magnetic properties at AP were measured with the Quantum Design Physical Property Measurement System (PPMS) and Magnetic Property Measurement System (MPMS-Ⅲ), respectively.

High-pressure transport and ac magnetic susceptibility were performed in the palm-type cubic anvil cell (CAC) apparatus with high hydrostatic pressures.[16,17] Standard four-probe method was employed for resistivity measurement with the current applied along the b-axis. As shown in the inset of Fig. 2, the sample is tilted in the Teflon cell of CAC in order to prevent it from rotating so as to protect the electrical contacts during compression. Thus, the angle between magnetic field and the b-axis is about 45°. The sample-1 size in CAC is about $0.10 \times 0.12 \times 0.55$ mm^3. AC magnetic susceptibility was measured by mutual induction method at a fixed frequency and the sample-2 size is about $0.30 \times 0.30 \times 0.25$ mm^3. The primary and secondary coils are made of enameled copper wires of 25 µm in diameter. Glycerol was employed as the pressure transmitting medium. The pressure values inside the CAC were determined from the superconducting transition of Pb at low temperatures. BeCu-type diamond anvil cell (DAC) with 300 µm flat was used to measure high-pressure resistance with KBr as the solid pressure transmitting medium. The sample-3 size is about $5.0\times5.0\times70\,\mu m^3$. The pressure in DAC was monitored at room temperature with the ruby fluorescence method. All the low-temperature experiments were performed in a ^{4}He refrigerated cryostat equipped with a 9 T superconducting magnet at the Synergic Extreme Condition User Facility (SECUF).

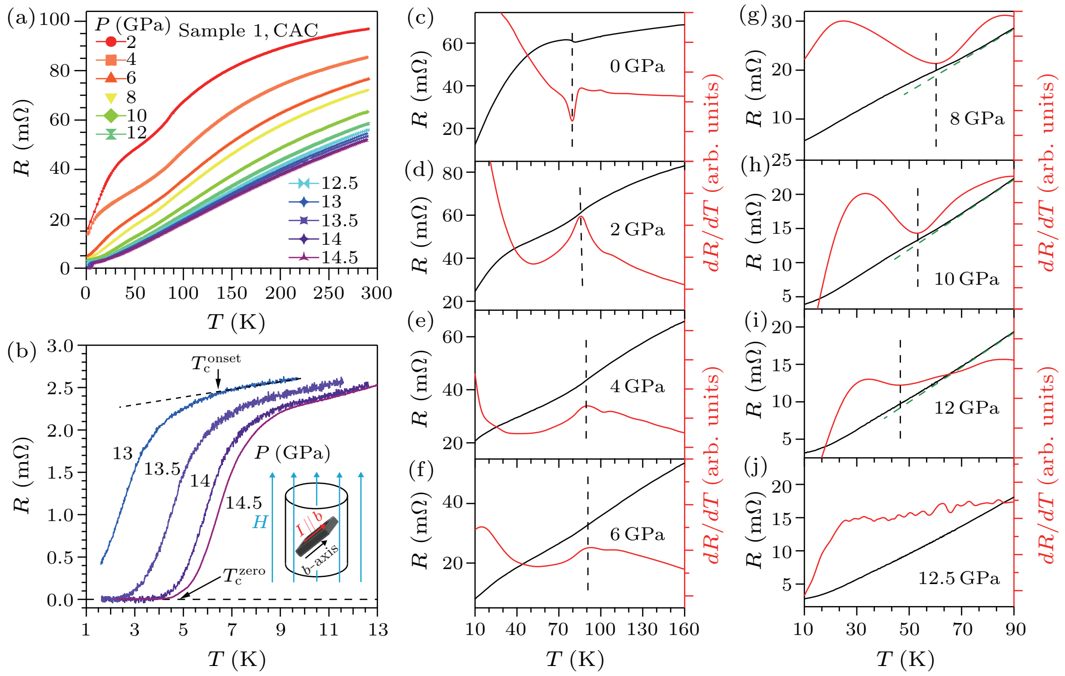

Fig. 2. (a) Electrical resistance of $RbMn_6Bi_5$ (sample 1) under various pressures measured in a CAC. (b) The low-temperature $R(T)$ data highlighting the superconducting transition. (c)–(j) The $R(T)$ and the corresponding dR/dT curve at each pressure showing the evolution of the antiferromagnetic transition.

Results. The $RbMn_6Bi_5$ crystals are black in color with metallic luster and have a needle shape with the longest dimension along the b-axis. They were first characterized at AP via measurements of electrical resistivity $\rho(T)$ and magnetic susceptibility $\chi(T)$ along the rod direction. As shown in Fig. 1(b), the $\rho(T)$ of $RbMn_6Bi_5$ shows a metallic behavior in the whole temperature range and exhibits a clear hump anomaly around 83 K, where a sudden drop in $\chi(T)$ appears. The estimated residual resistivity ratio [$\mathrm{RRR}\equiv\rho(300\,\mathrm{K})/\rho(2\,\mathrm{K})$] for the $RbMn_6Bi_5$ crystal is about 17, and the Curie–Weiss fitting to the paramagnetic susceptibility above 100 K yields an effective moment of $1.68\mu_B$/Mn. These values are close to those reported in literature.[10] It should be noted that the observed $\rho(T)$ is different from that reported in Ref. [10] along the b-axis. Here, the observed upturn feature indicates the inclusion of contribution from $\rho_\perp$. As shown in the inset of Fig. 1(b), the $RbMn_6Bi_5$ crystals are soft and are composed of a bundle of thin fibers, consistent with the Q1D character of the crystal structure. Such a character makes it easy to pick up the signal perpendicular to the b-axis when measuring resistivity of the bulk crystal with the standard four-probe configuration. Nonetheless, these measurements confirm the metallic nature of $RbMn_6Bi_5$ with an antiferromagnetic ordering transition at $T_N = 83$ K.

Figure 2(a) shows the resistance $R(T)$ data of $RbMn_6Bi_5$ crystal (sample 1) measured along the b-axis under various hydrostatic pressures up to 14.5 GPa in a CAC apparatus. The overall evolutions of $R(T)$ under high pressure are similar to those observed in KMn_6Bi_5.[5] At 2 GPa, the $R(T)$ shows a saturation behavior at high temperatures and a weak inflection point around T_N, followed by a broad hump at low temperatures. Here, T_N can be determined from the peak of dR/dT, Fig. 2(d). With increasing pressure, the resistance is reduced progressively and the features around T_N and below are weakened gradually; the T_N values determined from local maximum of dR/dT are enhanced slightly from 83 K at AP to ∼93 K at 6 GPa, Figs. 2(c)–2(f). Upon increasing pressure to 8 GPa, the $R(T)$ behaves differently, and the downward inflection feature around T_N evolves into a weak hump-like anomaly; the corresponding anomaly in dR/dT changes to a broad dip, Fig. 2(g). Similar crossover is also found in the resistance of KMn_6Bi_5 and may be associated with the modification of the antiferromagnetic structure under pressure and/or the emergence of spin density wave above 8 GPa in $RbMn_6Bi_5$. With further increasing pressure, the hump anomaly is weakened and T_N is reduced gradually, reaching ∼46 K at 12 GPa [Fig. 2(i)]. No clear anomaly can be discerned in the $R(T)$ of 12.5 GPa [Fig. 2(j)], indicating that the long-range antiferromagnetic order in $RbMn_6Bi_5$ has been suppressed completely.

Accompanying the collapse of antiferromagnetic order in $RbMn_6Bi_5$, we observed a sudden drop of resistance at low temperatures, signaling the possible occurrence of superconductivity. Here we define the onset and zero-resistivity temperatures of the superconducting transition, T_c^{onset} and T_c^{zero}, as the temperatures where the resistance starts to deviate from high-temperature linear extrapolation and reduces to nearly zero, respectively. As shown in Fig. 2(b), the $R(T)$ at 13 GPa starts to decrease at $T_c^{onset} \approx 6.6$ K, and zero resistance can be reached below $T_c^{zero} \approx 2.3$ K at 13.5 GPa. With increasing pressure, the superconducting transition moves to higher temperatures gradually; T_c^{onset} and T_c^{zero} at 14.5 GPa reach about 9.2 K and 4.3 K, respectively. The observed optimal T_c value of $RbMn_6Bi_5$ is close to that of KMn_6Bi_5 (∼ 9.3 K),[5] and is much higher than that of MnP (∼1 K).[4]

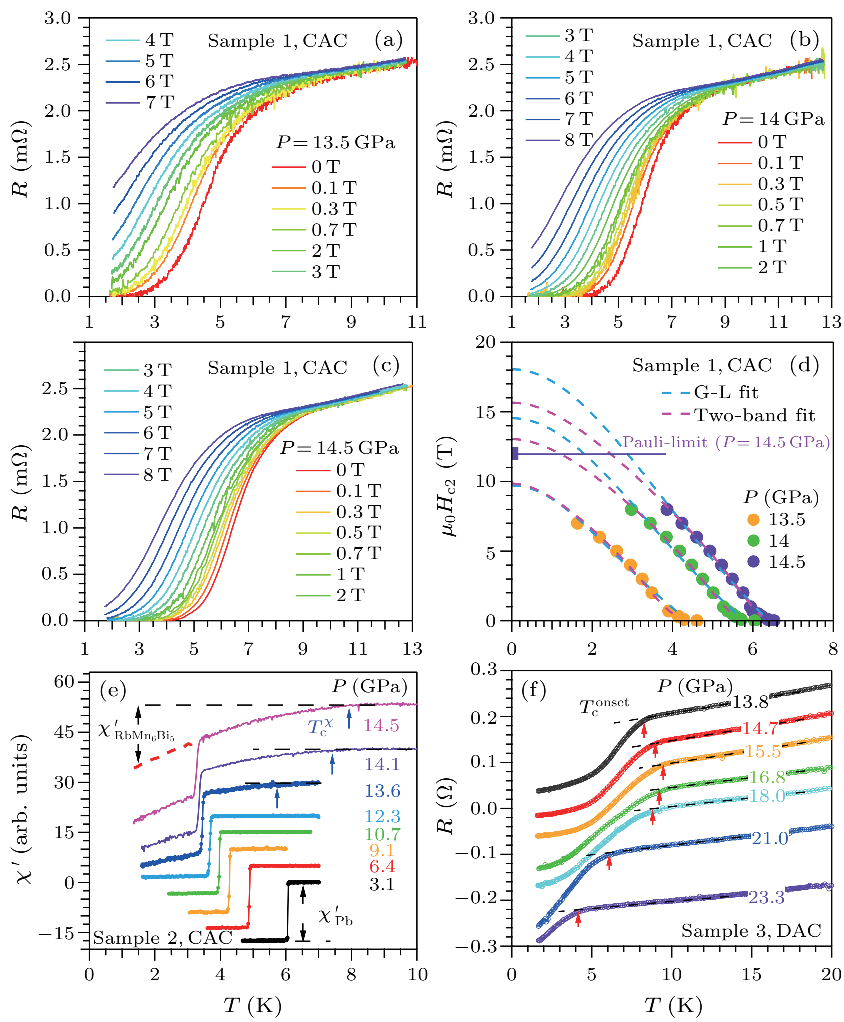

Fig. 3. (a)–(c) $R(T)$ under different magnetic fields at 13.5, 14 and 14.5 GPa. (d) The temperature dependences of $\mu_0 H_{c2}(T)$ fitted by the Ginzburg–Landau (G-L) equation, $\mu_0 H_{c2}(T) = \mu_0 H_{c2}(0)[1 - (T/T_c)^2]/[1 + (T/T_c)^2]$ and the two-band model. (e) The ac magnetic susceptibility $\chi'(T)$ of $RbMn_6Bi_5$ crystal (sample 2) and a piece of Pb with similar volume. (f) The low-temperature $R(T)$ data of $RbMn_6Bi_5$ crystal (sample 3) measured with a DAC. The curves in (e) and (f) have been shifted vertically for clarity.

To characterize the superconducting state, $R(T)$ under different magnetic fields were recorded at 13.5, 14, and 14.5 GPa for $RbMn_6Bi_5$. As shown in Figs. 3(a)–3(c), with increasing magnetic field the superconducting transition is shifted to lower temperatures and broadened up gradually owing to the magnetic-breaking effect and the flux creep effect in the vortex state. Here, we employed the criteria of 50% R_n to determine T_c at each field and plotted the temperature dependence of $\mu_0 H_{c2}(T)$ in

Fig. 3(d). The zero-temperature upper critical field $\mu_0 H_{c2}(0)$ is obtained by fitting the experimental data to the Ginzburg–Landau (G-L) equation, $\mu_0 H_{c2}(T) = \mu_0 H_{c2}(0)[1-(T/T_c)^2]/[1+(T/T_c)^2]$.[18] Then, the coherence length $\xi(0)$ can be calculated according to the relationship: $\mu_0 H_{c2}(0) = \Phi_0/2\pi\xi(0)^2$, where $\Phi_0 = h/2e = 2.067\times10^{-15}$ Wb is the magnetic flux quantum. As seen in Fig. 3(d), $\mu_0 H_{c2}(0)$ increases dramatically from 9.7 T at 13.5 GPa to 18.0 T at 14.5 GPa, the latter value being well above the Pauli limit of $\mu_0 H_p = 1.84 T_c = 11.1$ T.[19] Accordingly, the value of $\xi(0)$ decreases from 58.2 Å at 13.5 GPa to 47.5 Å at 14.5 GPa. The presences of large $\mu_0 H_{c2}(0)$ and small coherence length are the common features of unconventional superconductivity.[19,20]

We note that the $\mu_0 H_{c2}(T)$ curve displays a tail near 0 T, which cannot be well described by the simple G-L fitting, suggesting the presence of multi-band effect.[21,22] We thus also fit the data by adopting two-band model as shown in Fig. 3(d) and the estimated $\mu_0 H_{c2}(0)$ are about 9.85 T, 13.05 T and 15.66 T for 13.5 GPa, 14 GPa and 14.5 GPa, respectively. Although the obtained $\mu_0 H_{c2}(0)$ values with the two-band model are smaller than that obtained with G-L fitting, they still exceed the Pauli limit. In addition to the unconventional pairing mechanism, other effects such as the multi-band behavior, strong electronic correlations and strong coupling may also contribute to the observed large $\mu_0 H_{c2}(0)$ in $RbMn_6Bi_5$, which requires more studies in the future.

Figure 3(e) shows the ac magnetic susceptibility $\chi'(T)$ for $RbMn_6Bi_5$ crystal (sample 2) and a piece of Pb, which serves as a superconducting reference to estimate the superconducting shielding volume fraction of $RbMn_6Bi_5$. The pressure values in Fig. 3(e) were estimated based on the superconducting T_c of Pb. As can be seen, only the superconducting transition of Pb is observed at $P \le 12.3$ GPa, and the sharp transitions elaborate an excellent hydrostatic pressure environment in CAC. At $P \ge 13.6$ GPa, in addition to the sudden drop of $\chi'(T)$ for Pb, we observed a gradual reduction of $\chi'(T)$ below the superconducting critical temperature (T_c^{χ}) of $RbMn_6Bi_5$. In accordance with the resistance data shown in Fig. 2(b), T_c^{χ} also increases with pressure and reaches about 8 K at 14.5 GPa. The superconducting shielding volume fraction also increases with decreasing temperature, and reaches nearly 100% at 1.5 K, confirming the bulk nature of the observed superconductivity in $RbMn_6Bi_5$.

To track the evolution of the superconducting transition at higher pressures, we measured the $R(T)$ of $RbMn_6Bi_5$ crystal (sample 3) by using a diamond anvil cell (DAC) up to 23.3 GPa. Except for the $R(T)$ data at 13.8 GPa, other curves in Fig. 3(f) have been shifted down vertically for clarity. As seen in Fig. 3(f), the superconducting transition can be clearly detected as a drop of resistance below $T_c^{\rm onset}$, but the zero resistance cannot be achieved, presumably due to the non-hydrostatic pressure conditions in DAC employing a solid pressure transmitting medium. Similarly, the $T_c^{\rm onset}$ is defined where the resistance starts to deviate from the linear extrapolation. With increasing pressure in DAC, $T_c^{\rm onset}$ increases monotonously from ∼8.2 K at 13.8 GPa to a maximum of ∼9.5 K at 15.5 GPa, and then decreases gradually to ∼4.1 K at 23.3 GPa, giving rise to a superconducting dome as shown below. Concomitant with the reduction of T_c, the drop of resistance below T_c also becomes smaller.

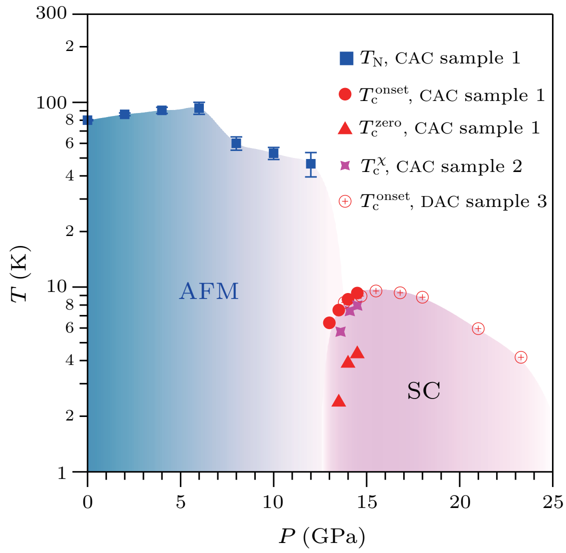

Fig. 4. T–P phase diagram of $RbMn_6Bi_5$. The AFM and SC refers to the antiferromagnetic and the superconducting phases, respectively.

Based on the above experimental results obtained using CAC and DAC, we can construct a T–P phase diagram for $RbMn_6Bi_5$ as summarized in Fig. 4. With increasing pressure, $T_N(P)$ first increases moderately from 83 K at AP to ∼93 K at 6 GPa, where it experiences a sudden drop and then decreases gradually until it vanishes abruptly at a critical pressure of $P_c \approx 13$ GPa. For most antiferromagnetic metals, $T_N(P)$ decreases monotonically with pressure. In the present case, the initial increase of T_N from AP to ∼6 GPa may be attributed to the enhanced intercolumn exchange interactions. The modification of relative strength of intercolumn to intracolumn interactions may alter the magnetic structure around 6 GPa, which then induces the changes of characteristic anomalies in $\rho(T)$ and $d\rho/dT$ around T_N. Such a crossover is similar to that observed recently in the Kagome metal CsV_3Sb_5 under pressure associated with an anisotropic lattice compressibility and modification of change density wave.[23] Bulk superconductivity emerges at about 13 GPa and zero-resistance state is achieved at 13.5 GPa. $T_c(P)$ increases monotonously to a maximal value of $T_c^{\rm onset} \approx$

9.5 K at 15.5 GPa and then decreases gradually with further increasing pressures. These features define a pressure-induced superconducting dome on the border of long-range antiferromagnetically ordered state (see Fig. 4). Such a T–P phase diagram of $RbMn_6Bi_5$ is almost identical to that of KMn_6Bi_5 and resembles those of many unconventional superconducting systems associated with magnetism-mediated pairing mechanism.[6–8,20]

Discussions. The discovery of pressure-induced superconductivity with a relatively high $T_c \approx 9$ K in the Q1D materials (K/Rb)Mn_6Bi_5 is quite encouraging and will stimulate more studies in related Mn-based superconductors.

Firstly, (K/Rb)Mn_6Bi_5 represent a new class of *ternary* Mn-based superconductors with unique Q1D crystal structure and possible novel $[Mn_6Bi_5]^-$ superconducting gene. As mentioned above, the Mn-based superconductors are quite rare owing to the strong magnetic pair-breaking effect. So far, pressure-induced superconductivity has been observed only in the *binary* MnP and MnSe.[4,24] In these cases, other tuning methods expect for applying pressure are less effective in regulating the magnetism and inducing superconductivity so far. In contrast, the *ternary* $A$$Mn_6Bi_5$ with a flexible Q1D structure provides more possibilities to tune the physical properties at AP, e.g., via carrier doping or chemical substitutions at the A- and/or Bi-sites.

Secondly, they offer a new material platform to study the interplay between exotic magnetism and superconductivity. The magnetic structure of $A$$Mn_6Bi_5$ has not been resolved experimentally. According to the density-functional-theory calculations, $RbMn_6Bi_5$ could adopt a complex helical antiferromagnetic structure at AP.[10] As pointed out previously for MnP,[4,25] the emergence of superconductivity in a helical magnet is rare; it deserves in-depth studies to understand the role of spin fluctuations associated with helical order in driving superconductivity. In this regard, it is highly desirable to determine the magnetic structure of $A$$Mn_6Bi_5$ at AP and then to reveal its evolution under high pressures. In addition, the information about the spin dynamics near the antiferromagnetic QCP around P_c are also important to understand the superconducting mechanism.

Thirdly, considering the fact that the observed large $\mu_0H_{c2}(0)$ exceeds the Pauli paramagnetic limit, it is interesting to investigate the superconducting pairing mechanism. For example, spin-triplet superconducting state has been proposed and verified by the nuclear magnetic resonance (NMR) experiments in the Q1D superconductor $A_2Cr_3As_3$, which possesses a similar crystal structure and unusually large $\mu_0H_{c2}(0)$.[15,26,27] Thus, the NMR experiments under high pressure on (K/Rb)Mn_6Bi_5 are highly desirable to investigate the superconducting gap symmetry.

Last but not least, although the Mn-based compounds are commonly believed to be antagonistic to superconductivity and thus should have a low T_c, the present work demonstrates that the transition temperature of Mn-based superconductors can be raised at least to the level of 10 K. Our work thus calls for more investigations on $A$$Mn_6Bi_5$ and other complex Mn-based compounds with an aim to further raise the T_c of Mn-based superconductors.

In summary, we report the discovery of superconductivity on the border of antiferromagnetic order in the Q1D $RbMn_6Bi_5$ under pressure. Bulk superconductivity emerges and display a superconducting dome with the maximal $T_c^{\rm onset} \approx 9.5$ K at about 15 GPa. The constructed T–P phase diagram and the usually large upper critical field $\mu_0H_{c2}(0)$ exceeding the Pauli paramagnetic limit suggest an unconventional superconducting paring mechanism for $RbMn_6Bi_5$. Along with our recent work on KMn_6Bi_5, the present study establishes that $A$$Mn_6Bi_5$ (A = alkali metal) represent a new family of ternary Mn-based superconductors with relatively high T_c. More studies are needed to reveal the complex magnetism and its relationship with the observed superconductivity.

Acknowledgements. This work was supported by the Beijing Natural Science Foundation (Grant No. Z190008), the National Key R&D Program of China (Grant Nos. 2018YFA0305700 and 2021YFA1400200), the National Natural Science Foundation of China (Grant Nos. 12025408, 11874400, 11834016, 11921004, 11904391, 12174424, and 11888101), the Strategic Priority Research Program and Key Research Program of Frontier Sciences of CAS (Grant Nos. XDB25000000, XDB33000000 and QYZDB-SSW-SLH013), the CAS Interdisciplinary Innovation Team (Grant No. JCTD-201-01), K. C. Wong Education Foundation (GJTD-2020-01), the Users with Excellence Program of Hefei Science Center CAS (Grant No. 2021HSC-UE008), Youth Promotion Association of CAS (Grant No. 2018010), and Y.U. acknowledges the support from JSPS KAKENHI (Grant No. JP19H00648).

References

[1] Bednorz J G and Müller K A 1986 *Z. Phys. B: Condens. Matter* **64** 189

[2] Kamihara Y, Hiramatsu H, Hirano M, Kawamura R, Yanagi H, Kamiya T and Hosono H 2006 *J. Am. Chem. Soc.* **128** 10012

[3] Kamihara Y, Watanabe T, Hirano M and Hosono H 2008 *J. Am. Chem. Soc.* **130** 3296

[4] Cheng J G, Matsubayashi K, Wu W, Sun J P, Lin F K, Luo J L and Uwatoko Y 2015 *Phys. Rev. Lett.* **114** 117001

[5] Liu Z Y, Dong Q X, Yang P T, Shan P F, Wang B S, Sun J P, Uwatoko Y, Chen G F, Dong X L, Zhao Z X and Cheng

J G 2022 *Phys. Rev. Lett.* **128** 117001
[6] Gegenwart P, Si Q and Steglich F 2008 *Nat. Phys.* **4** 186
[7] Stewart G R 2011 *Rev. Mod. Phys.* **83** 1589
[8] Keimer B, Kivelson S A, Norman M R, Uchida S and Zaanen J 2015 *Nature* **518** 179
[9] Bao J K, Tang Z T, Jung H J, Liu J Y, Liu Y, Li L, Li Y K, Xu Z A, Feng C M, Chen H, Chung D Y, Dravid V P, Cao G H and Kanatzidis M G 2018 *J. Am. Chem. Soc.* **140** 4391
[10] Chen L, Zhao L, Qiu X, Zhang Q, Liu K, Lin Q and Wang G 2021 *Inorg. Chem.* **60** 12941
[11] Zhou Y, Chen L, Wang G, Wang Y X, Wang Z C, Chai C C, Guo Z N, Hu J P and Chen X L 2022 *Chin. Phys. Lett.* **39** 047401
[12] Matsuda M, Ye F, Dissanayake S E, Cheng J G, Chi S, Ma J, Zhou H D, Yan J Q, Kasamatsu S, Sugino O, Kato T, Matsubayashi K, Okada T and Uwatoko Y 2016 *Phys. Rev. B* **93** 100405(R)
[13] Taddei K M, Xing G, Sun J, Fu Y, Li Y, Zheng Q, Sefat A S, Singh D J and de la Cruz C 2018 *Phys. Rev. Lett.* **121** 187002
[14] Cuono G, Forte F, Romano A, Ming X, Luo J, Autieri C and Noce C 2021 *Phys. Rev. Mater.* **5** 064402
[15] Bao J K, Liu J Y, Ma C W, Meng Z H, Tang Z T, Sun Y L, Zhai H F, Jiang H, Bai H, Feng C M, Xu Z A and Cao G H 2015 *Phys. Rev. X* **5** 011013
[16] Uwatoko Y, Matsubayashi K, Matsumoto T, Aso N, Nishi M, Fujiwara T, Hedo M, Tabata S, Takagi K, Tado M and Kagi H 2008 *Rev. High Pressure Sci. Technol.* **18** 230
[17] Cheng J G, Matsubayashi K, Nagasaki S, Hisada A, Hirayama T, Hedo M, Kagi H and Uwatoko Y 2014 *Rev. Sci. Instrum.* **85** 093907
[18] Tinkham M 1963 *Phys. Rev.* **129** 2413
[19] Clogston A M 1962 *Phys. Rev. Lett.* **9** 266
[20] Lee P A, Nagaosa N and Wen X G 2006 *Rev. Mod. Phys.* **78** 17
[21] Gurevich A 2003 *Phys. Rev. B* **67** 184515
[22] Hunte F, Jaroszynski J, Gurevich A, Larbalestier D C, Jin R, Sefat A S, McGuire M A, Sales B C, Christen D K and Mandrus D 2008 *Nature* **453** 903
[23] Chen K Y, Wang N N, Yin Q W, Gu Y H, Jiang K, Tu Z J, Gong C S, Uwatoko Y, Sun J P, Lei H C, Hu J P and Cheng J G 2021 *Phys. Rev. Lett.* **126** 247001
[24] Hung T L, Huang C H, Deng L Z, Ou M N, Chen Y Y, Wu M K, Huyan S Y, Chu C W, Chen P J and Lee T K 2021 *Nat. Commun.* **12** 5436
[25] Norman M 2015 *Physics* **8** 24
[26] Wu X, Yang F, Le C, Fan H and Hu J 2015 *Phys. Rev. B* **92** 104511
[27] Yang J, Luo J, Yi C, Shi Y, Zhou Y and Zheng G Q 2021 *Sci. Adv.* **7** eabl4432